Rapid measurement of long-range distances in proteins by multidimensional 13C–19F REDOR NMR under fast magic-angle spinning

Published in final edited form as:

J Biomol NMR. 2018 May ; 71(1): 31–43. doi:10.1007/s10858-018-0187-0.

Rapid Measurement of Long-Range Distances in Proteins by Multidimensional ^{13}C-^{19}F REDOR NMR under Fast Magic-Angle Spinning

Alexander A. Shcherbakov and **Mei Hong**

Department of Chemistry, Massachusetts Institute of Technology, 170 Albany Street, Cambridge, MA 02139

Abstract

The ability to simultaneously measure many long-range distances is critical to efficient and accurate determination of protein structures by solid-state NMR (SSNMR). So far, the most common distance constraints for proteins are ^{13}C-^{15}N distances, which are usually measured using the rotational-echo double-resonance (REDOR) technique. However, these measurements are restricted to distances of up to ~5 Å due to the low gyromagnetic ratios of ^{15}N and ^{13}C. Here we present a robust 2D ^{13}C-^{19}F REDOR experiment to measure multiple distances to ~10 Å. The technique targets proteins that contain a small number of recombinantly or synthetically incorporated fluorines. The ^{13}C-^{19}F REDOR sequence is combined with 2D ^{13}C-^{13}C correlation to resolve multiple distances in highly ^{13}C-labeled proteins. We show that, at the high magnetic fields that are important for obtaining well resolved ^{13}C spectra, the deleterious effect of the large ^{19}F chemical shift anisotropy (CSA) for REDOR is ameliorated by fast magic-angle spinning (MAS) and is further taken into account in numerical simulations. We demonstrate this 2D ^{13}C-^{13}C resolved ^{13}C-^{19}F REDOR technique on ^{13}C, ^{15}N-labeled GB1. A 5-^{19}F-Trp tagged GB1 sample shows the extraction of distances to a single fluorine atom, while a 3-^{19}F-Tyr labeled GB1 sample allows us to evaluate the effects of multi-spin coupling and statistical ^{19}F labeling on distance measurement. Finally, we apply this 2D REDOR experiment to membrane-bound influenza BM2 transmembrane peptide, and show that the distance between the proton-selective histidine residue and the gating tryptophan residue differs from the distances in the solution NMR structure of detergent-bound BM2. This 2D ^{13}C-^{19}F REDOR technique should facilitate SSNMR-based protein structure determination by increasing the measurable distances to the ~10 Å range.

Introduction

Long-range inter-atomic distances are valuable restraints in NMR-based structure determination. In magic-angle-spinning (MAS) solid-state NMR, the rotational-echo double-resonance (REDOR) experiment (Gullion and Schaefer 1989; Pan et al. 1990) is one of the most robust methods for recoupling heteronuclear dipolar interactions and quantifying distances. Since its introduction nearly 30 years ago, REDOR has been applied to many spin-1/2 and quadrupolar nuclei (Cegelski 2013). In biomolecular systems, the most

Corresponding author: Mei Hong, meihong@mit.edu.

commonly exploited nuclear spins are ^{1}H, ^{19}F, ^{31}P, ^{13}C, ^{15}N, ^{2}H, among which ^{1}H and ^{19}F hold the most promise for giving long-range distances because of their high gyromagnetic ratios. Indeed, REDOR experiments between ^{19}F and other nuclei such as ^{31}P and ^{13}C have been exploited (Goetz et al. 1999; Graesser et al. 2007; Kim et al. 2006; Mani et al. 2006a; Mani et al. 2006b), and REDOR between ^{1}H and other spins have also been demonstrated (Ghosh and Rienstra 2017; Hong and Schmidt-Rohr 2013; Sinha and Hong 2003; Wi et al. 2004). For example, ^{1}H-^{19}F REDOR has been used to measure a distance of 7.7 Å in a model peptide at MAS frequencies of < 10 kHz (Wi et al. 2004), where ^{1}H-^{1}H homonuclear decoupling was used to lengthen the ^{1}H transverse relaxation time to observe sufficiently weak dipolar dephasing.

Recently, we showed that biosynthetic incorporation of a small number of fluorine atoms into proteins allows the measurement of multiple ^{19}F-^{19}F distances to ~1.6 nm (Roos et al. 2018). These sparse ^{19}F spins also serve as probes to dephase the surrounding ^{13}C and ^{15}N nuclei through commuting dipole-dipole interactions, and hence should permit the measurement of many ^{13}C-^{19}F and ^{15}N-^{19}F distances. However, at the high magnetic fields that are commonly used for protein structure determination, the chemical shift anisotropy (CSA) of aromatic fluorines can be as large as ~50 kHz, which easily exceeds the ^{13}C-^{19}F dipolar coupling of interest by two orders of magnitude. The effects of this large CSA on REDOR have not been investigated. When fast MAS is used to reduce the number of ^{19}F spinning sidebands and to obtain high-resolution ^{13}C and ^{15}N spectra, the fraction of the rotor periods occupied by the REDOR 180° pulses increases, which slows down dipolar dephasing (Jaroniec et al. 2000; Sack et al. 1999). Moreover, under fast MAS, a large number of ^{19}F pulses are required to reach sufficiently long mixing times to measure weak dipolar couplings and long distances. The cumulative pulse imperfections are expected to reduce the accuracy of the REDOR technique. These potential difficulties need to be investigated and addressed before ^{13}C-^{19}F REDOR can be practically useful at high magnetic fields under fast MAS.

Here we demonstrate a 2D ^{13}C-^{13}C resolved ^{13}C-^{19}F REDOR experiment to measure multiple long-range distances in proteins. We use the 56-residue GB1 (Franks et al. 2005) and the tripeptide formyl-MLF (Hong and Griffin 1998; Rienstra et al. 2002) as our model compounds, and show that ^{13}C-^{19}F REDOR is effective at spinning rates of 25–40 kHz, for aromatic ^{19}F CSA's up to ~40 kHz at the magnetic field strength of 14.1 Tesla. We show that ^{13}C-^{19}F distances can be quantified with reasonable precision using a simple two-spin model, as long as the fluorine spins are well separated from each other. Finally, we apply this 2D ^{13}C-^{13}C resolved ^{13}C-^{19}F distance experiment to membrane-bound influenza B M2 transmembrane peptide (Williams et al. 2017; Williams et al. 2016), and show that ^{13}C-^{19}F dipolar dephasing between the proton-selective histidine and the gating tryptophan indicates significantly different sidechain structures from the micelle-bound BM2 structure.

Materials and Methods

Preparation of fluorinated peptides and proteins

Five fluorinated samples were used in this study. Two formyl-MLF peptides with different labeling schemes were used: the first sample contains 4-^{19}F-Phe and ^{13}CO-labeled Leu (Wi

et al. 2004) and was used for 1D ^{13}C-^{19}F REDOR experiments, while the second sample (Biopeptek Pharmaceuticals, Malvern, PA) contains CF_3-Met, uniformly ^{13}C, ^{15}N-labeled Leu, and 4-^{19}F-Phe, and was used for measuring ^{19}F chemical shift anisotropies (Roos et al. 2018). Two ^{13}C, ^{15}N-labeled GB1 samples were used for measuring 2D REDOR-RFDR spectra: one sample contains 3-^{19}F-labeled Tyr3, Tyr33, and Tyr45 (3F-Tyr GB1), while the other sample contains 5-^{19}F labeled Trp43 (5F-Trp GB1). The fifth sample is the influenza B virus M2 (BM2) transmembrane (TM) peptide (residues 1–33), which contains uniformly ^{13}C, ^{15}N-labeled S12, A17, H19, G26, and 5-^{19}F-Trp23 (Williams et al. 2017; Williams et al. 2016). The peptide was bound to a virus-mimetic membrane (VM+) (Cady et al. 2011; Luo et al. 2009) at pH 5.5 at a peptide/lipid molar ratio of 1 : 13.3.

^{13}C, ^{15}N and fluorinated GB1 samples were expressed in BL21 (DE3) *E. coli* cells. After cells were grown to OD_{600} = 0.5 in M9 media containing ^{13}C-labeled glucose and ^{15}N-labeled ammonium chloride, we added glyphosate to a final concentration of 1 g/L to suppress the pentose phosphate pathway for aromatic amino acid synthesis (Lehninger et al. 1993). Immediately after glyphosate addition, we added aromatic amino acids with different combinations of fluorinated residues. For the 3F-Tyr-labeled GB1, 50 mg each of 3F-L-Tyr, unlabeled L-Phe and unlabeled L-Trp were added to the M9 media to give a final concentration of 100 mg/L. For 5F-Trp labeled GB1, 50 mg each of 5F-L-Trp, unlabeled L-Tyr and L-Phe were added. Each aromatic amino acid was first dissolved in 5 mL M9 media before being added to the culture, in order to facilitate rapid uptake of the amino acids by the cells. Following incubation for 30 minutes, when OD_{600} reached 0.6, we added 0.5 mM isopropyl β-D-thiogalactoside (IPTG) to initiate protein expression. Proteins were purified by size-exclusion chromatography using a HiLoad 26/60 Superdex 75 prep grade column (GE) in pH 7.0 phosphate buffer containing 100 mM NaCl. The protein was then dialyzed to remove sodium chloride, then concentrated to 30 mg/mL using centrifugal concentrator devices (Millipore) with a 3,000 Da molecular weight cut-off under 5,000 g at 4°C. The concentrated protein was crystallized in pH 5.5 phosphate buffer using 2-methyl-2, 4-pentanediol (MPD) and isopropanol 2 : 1 v/v (Franks et al. 2005). The 3F-Tyr incorporation level was found to be ~95% by ESI and MALDI-TOF mass spectrometry, and the 5F-Trp incorporation level was verified by ESI-MS to be >95%.

For 3F-Tyr labeled GB1, each tyrosine is mono-fluorinated at the position *ortho*- to the hydroxyl group; however the 3-^{19}F and 5-^{19}F positions are indistinguishable during incorporation into the protein, thus the two positions are equally statistically occupied to 50% by a ^{19}F. For simplicity, we still designate this sample as 3F-Tyr GB1, although either the 3- or 5- position is fluorinated.

Solid-state NMR experiments

All solid-state NMR experiments were carried out on a Bruker Avance III HD spectrometer operating at a magnetic field of 14.1 Tesla, corresponding to Larmor frequencies of 600.10 MHz for ^{1}H, 564.66 MHz for ^{19}F, and 150.90 MHz for ^{13}C. A 1.9 mm HFX MAS probe with a maximum MAS frequency of 42 kHz was used. Chemical shifts were externally referenced to the 38.48 ppm CH_2 resonance of adamantane on the tetramethylsilane scale for ^{13}C, and to the −122.1 ppm signal of 5-^{19}F-Trp on the CF_3Cl scale (Dürr et al. 2008).

Typical ^{1}H radiofrequency (rf) field strengths were 71.4 kHz for excitation, 10 kHz for low-power WALTZ-16 decoupling, and 100–130 kHz for high-power TPPM decoupling (Bennett et al. 1995). RF field strengths for ^{19}F were 100 kHz for direct-polarization (DP) experiments and 71 kHz for REDOR 180° pulses. ^{13}C hard-pulse field strengths were 62 – 71 kHz, while the ^{13}C Gaussian 180° pulse field strengths were 1.56 – 3.13 kHz. Recycle delays were 1.5 – 2.0 s for CP-based experiments and 7.0 – 9.0s for DP experiments. Most REDOR spectra were measured under 25 kHz MAS, but additional GB1 spectra were also measured under 40 kHz MAS. ^{1}H – ^{13}C cross polarization (CP) used a spin-lock time of 1 ms, a 70 – 100% ramp on the ^{13}C channel, with Hartmann-Hahn matching to centerband condition (62.5 or 71.4 kHz) in the middle of the ramp (85%).

1D ^{13}C-^{19}F REDOR experiments were conducted on 4F-Phe labeled formyl-MLF to investigate the effectiveness of ^{13}C-^{19}F REDOR in the presence of large ^{19}F CSAs. A ^{13}C 180° pulse of 7 μs was applied to refocus the ^{13}C chemical shift during the REDOR mixing period (Fig. 1A). The ^{19}F carrier frequency was placed on resonance with the −115.9 ppm 4F-Phe peak to maximally invert the 4-^{19}F-Phe signal. The ^{19}F rf field strength was 62.5 kHz. ^{19}F 180° pulses used XY-4 phase cycling while the ^{13}C 180° pulse used the EXORCYCLE scheme to compensate for pulse flip-angle errors (Sinha et al. 2004). At 25 kHz MAS, ^{1}H TPPM decoupling was 120 kHz during the REDOR period and 100–120 kHz during acquisition to maximize ^{13}C T_2 and to obtain high-resolution ^{13}C spectra.

2D ^{13}C-^{13}C REDOR-RFDR experiments were implemented using the pulse sequence in Fig. 1B. A frequency-selective REDOR period was inserted before ^{13}C t_1 evolution. The ^{13}C Gaussian 180° pulse length was 320 μs for the GB1 spectra, and 240 μs and 160 μs for the BM2 Cα- and CO-selective spectra, respectively. The MAS rates of 25 and 40 kHz were sufficiently high that ^{13}C coherences outside the frequency-selected region have long T_2 relaxation times. These undesired coherences were removed by phase-cycling the ^{13}C Gaussian 180° pulse following the EXORCYCLE scheme. The ^{13}C RFDR (Bennett et al. 1998) mixing period was 2 ms to detect one-bond cross peaks, and the ^{13}C signals were detected after a Hahn echo to obtain undistorted baselines. Two 2D experiments, without (S_0) and with (S) ^{19}F recoupling pulses, were conducted to measure the T_2-corrected REDOR dipolar dephasing, S/S_0. ^{19}F recoupling field strengths were 71 kHz in the REDOR-RFDR experiments. For 5F-Trp GB1, REDOR mixing times of 6.4, 9.6, and 10.8 ms were measured, while for 3F-Tyr GB1, REDOR mixing times were 6.4 and 8.4 ms. For the influenza BM2 sample, REDOR mixing times were 4.0 and 6.4 ms. ^{1}H decoupling field strengths of 100–130 kHz were used for experiments at 25 kHz MAS. 2D REDOR-RFDR spectra of GB1 were acquired with 64 – 128 scans per t_1 point and 512 t_1 points. BM2 spectra were acquired with 256 scans and 144 t_1 increments.

REDOR simulations

REDOR simulations were performed using the SIMPSON software (Bak et al. 2000). Powder averaging used the REPULSION320 scheme with 64 γ angles (Bak and Nielsen 1997). Simulations to explore the effects of CSA on REDOR dephasing employed a two-spin system with a 6 Å distance, corresponding to a dipolar coupling constant of 132 Hz. The ^{19}F CSA used in the REDOR simulations were measured from the 1D ^{19}F spinning

sideband spectra using TopSpin's Solids Lineshape Analysis module (Fig. S1) (Roos et al. 2018). All REDOR simulations used finite ^{19}F and ^{13}C 180° pulses that match the experimental pulse lengths.

For 4F-Phe formyl-MLF, ^{19}F pulse angle imperfection was taken into account by adding a scaling factor to the ^{19}F rf field strength to give effective flip angles of 180° to 145° in 5° increments. The simulations for different ^{19}F pulse angles were added using weights that match a normal distribution centered at 180° with a standard deviation of 15°. The weighted average S/S_0 curves were calculated for ^{13}C-^{19}F distances of 4.0 to 9.0 Å in 0.5 Å increments. To average over a distribution of distances, flip-angle distributed simulations for different distances were added using coefficients from a normal distribution centered at 6.5 Å with a standard deviation of 1.5 Å. The data for 5F-Trp were analyzed using the same flip-angle distribution, but without distance distribution. Data for 3F-Tyr GB1 and BM2 samples did not consider a distribution of flip angles, since complicating factors of multiple ^{19}F dephasers and lower spectral sensitivity obscure these effects.

The random uncertainties σ_{S/S_0} in the REDOR S/S_0 values at each mixing time were propagated from the signal-to-noise ratios (SNR) of the S_0 and S spectra using the equation:

$$\sigma_{S/S_0} = \frac{S}{S_0}\left(\frac{1}{(SNR_S)^2} + \frac{1}{\left(SNR_{S_0}\right)^2}\right)^{1/2} \quad (1)$$

Root-mean-square deviations (RMSDs) between the measured and simulated REDOR S/S_0 values were calculated in MATLAB. Any distances whose simulated REDOR curves agree with the experimental data with an RMSD below the average experimental uncertainty are considered to be consistent with the data. In cases where the S/S_0 values at the longest mixing time are relatively high and do not distinguish multiple simulated REDOR decay curves, the upper bound of the measured distance cannot be determined.

Results

^{19}F chemical shift anisotropies in proteins and their influence on ^{13}C-^{19}F REDOR dephasing

The main difference between REDOR of low-frequency spin-1/2 nuclei and ^{13}C-^{19}F REDOR is the large isotropic and anisotropic chemical shifts of the ^{19}F spins. In combination with the large gyromagnetic ratio of ^{19}F, this results in a very wide ^{19}F spectral width, which is difficult to invert fully unless strong rf fields are applied. As an example, Fig. 2 shows the ^{19}F MAS spectra of GB1 and formyl-MLF, which include both aromatic fluorines and a trifluoromethyl (CF_3) group. Under 25 kHz MAS, significant sideband intensities are detected for 3F-Tyr residues in GB1, and only at 40 kHz MAS are most sidebands suppressed, as shown for 4-^{19}F-Phe in formyl-MLF. These spectra show a large isotropic shift dispersion of ~100 ppm between CF_3 and CF groups: in formyl MLF the Met CF_3 peak resonates at −38.9 ppm, with a full-width at half maximum (FWHM) of 0.53 ppm,

while the 4F-Phe peak resonates at −115.9 ppm with a FWHM of 1.4 ppm. This isotropic chemical shift difference corresponds to 43.5 kHz at 14.1 Tesla. The 3F-Tyr peaks in GB1 resonate even more upfield than 4F-Phe, at about −135 ppm. Therefore ^{13}C-^{19}F REDOR experiments must either use strong ^{19}F radiofrequency pulses for broadband inversion or employ frequency-selective approaches. ^{19}F spinning sideband spectra measured under slow MAS rates indicate a chemical shift anisotropy (CSA) parameter (δ_{zz}-δ_{iso}) of −59 ppm for 4F-Phe, while Met CF_3 has a motionally averaged CSA of +17 ppm (Fig. S1). For the three 3F-Tyr residues in GB1, the isotropic shift range is small, about 3 ppm (Fig. 2A), and the linewidths were 0.3 ppm for this microcrystalline protein. Y3 and Y45, which are located in two β-strands, show CSAs of −75 ppm while the α-helical Y33 has a motionally averaged CSA of −58 ppm.

To investigate how the large ^{19}F CSAs affect REDOR dephasing, and to determine the optimal MAS rate and rf field strength required to obtain undistorted REDOR curves, we simulated ^{13}C-^{19}F REDOR curves for various combinations of ^{19}F CSA, MAS rate, and ^{19}F rf field strengths (Fig. 3). When the MAS rate is smaller than the ^{19}F CSA, the REDOR S/S_0 values shift up compared to the ideal values, and this deleterious effect is amplified by weak ^{19}F rf fields. These observations indicate incomplete recoupling for internuclear vectors that are oriented roughly parallel to the magnetic field. Increasing the MAS frequency to 50 kHz (Fig. 3B) resulted in lower S/S_0 values and hence more ideal dipolar dephasing, with minimum S/S_0 values close to 0. Under this condition, weaker ^{19}F rf pulses only slow down the dipolar dephasing moderately, due to the known finite pulse-length effect (Jaroniec et al. 2000). Fig. 3C–F further illustrate why fast MAS is important for overcoming the influence of the large ^{19}F CSA on REDOR dipolar dephasing. Under slow MAS, the REDOR dephasing curve does not have a monotonic dependence on the CSA, but deviates significantly from the ideal curve when the CSA exceeds the MAS rate by 2-fold. Increasing the MAS rate to above the CSA removes most of this effect and restores nearly ideal REDOR dephasing, other than the finite pulse-length effect.

Taken together, these simulations show that fast MAS is important for producing accurate REDOR dephasing curves at high magnetic fields. An aromatic ^{19}F CSA of −75 ppm, which is found for Y3 and Y45 in GB1, corresponds to a frequency of −42 kHz on the 600 MHz NMR spectrometer. Therefore, MAS frequencies above ~35 kHz are advisable. In practice, this consideration is moderated by the fact that fast MAS requires more ^{19}F pulses to reach the long mixing times necessary for measuring weak dipolar couplings, and the cumulative pulse imperfection will reduce the performance of the REDOR experiments.

^{13}C-^{19}F REDOR experiment of formyl-MLF

To investigate the effectiveness of ^{13}C-^{19}F REDOR under fast MAS, we measured 1D ^{13}C-^{19}F REDOR spectra of ^{13}CO-Leu, 4-^{19}F-Phe labeled formyl-MLF (Hong and Griffin 1998; Rienstra et al. 2002) under 25 kHz MAS. With the ^{19}F carrier frequency on resonance with the 4F-Phe peak, the Leu ^{13}CO signal shows dipolar dephasing to ~0.4 by 11.2 ms (Fig. 4A, B). Based on the structure of formyl-MLF (PDB code: 1Q7O), Leu ^{13}CO is 6.5 Å from 4-^{19}F of Phe, which corresponds to a coupling constant of 104 Hz. The ideal REDOR curve for this coupling, in the absence of large ^{19}F CSA, should exhibit a minimal S/S_0 at ~17 ms.

The measured data show much higher S/S_0 values, indicating the effects of the ^{19}F CSA and pulse imperfections. We took into account the ^{19}F CSA and ^{19}F pulse-length imperfections when simulating the REDOR curves. To account for rf field inhomogeneity and pulse flip-angle errors, we assumed a symmetric Gaussian distribution of ^{19}F flip angles centered at 180° with a standard deviation of 15° (Sinha et al. 2004). However, even with this flip-angle distribution, single-distance simulations still did not reproduce the experimental data well. Since the formyl-MLF structure (PDB: 1Q7O) shows moderate disorder in the Phe ring position due to a distribution of χ_1 torsion angles, we next adopted a Gaussian distribution of ^{13}CO-^{19}F distances centered at 6.5 Å with a standard deviation of 1.5 Å. With this distance distribution, the simulated REDOR curve agrees well with the measured dephasing, as shown in Fig. 4B.

2D ^{13}C-^{13}C resolved ^{13}C-^{19}F REDOR spectra of GB1

3F-Tyr GB1 represents a good model system for multiply fluorinated proteins in which distances to the ^{19}F spins need to be resolved in 2D or 3D correlation spectra. We measured 2D ^{13}C-^{13}C REDOR-RFDR spectra using the pulse sequence of Fig. 1B to demonstrate this approach. The triply labeled 3F-Tyr GB1 exhibits three levels of complexity, which are expected to be common in fluorinated proteins. First, the ^{19}F isotropic chemical shift range is relatively small, only 3 ppm. Second, both 3F and 5F are statistically equally incorporated, thus distances to both Hε1 and Hε2 need to be considered in the distance analysis. Third, if a Tyr sidechain undergoes fast reorientation, the REDOR dipolar dephasing will be partially averaged. Below we show that the three Tyr residues in GB1 exhibit both static and dynamic averaging, but we can still obtain distances with reasonable precision due to the sparseness of the ^{19}F incorporation, the long distances of the fluorines to many ^{13}C spins, and direct knowledge of sidechain motion from 1D ^{19}F spectra.

We first investigated whether fluorination of three Tyr residues perturbs the protein structure. A 2D ^{13}C-^{13}C RFDR spectrum with 4.8 ms mixing gave nearly identical ^{13}C chemical shifts (Fig. S2, S3) as non-fluorinated GB1 (Franks et al. 2005; Wylie et al. 2011), with a root-mean-square deviation of only 0.53 ppm (Table S1), indicating that biosynthetic incorporation of three fluorines does not perturb the global structure. Fig. 5 shows the 2D ^{13}C-^{19}F REDOR-RFDR spectra of GB1, measured under 25 kHz MAS with a REDOR mixing time of 8.4 ms and an RFDR mixing time of 2.08 ms. The shorter RFDR mixing time was used to obtain only one-bond correlations to reduce spectral congestion. The ^{13}C carrier frequency was placed at 56.2 ppm, thus the soft Gaussian pulse selectively refocuses the Cα chemical shifts in the indirect dimension. The 2D S_0 control spectrum has a different intensity distribution from the 2D RFDR spectrum with REDOR due to the ^{13}C selective inversion, while T_2-induced signal loss was negligible at the REDOR mixing time of 8.4 ms. After subtracting the dephased (S) spectrum (data not shown) from the S_0 spectrum, we obtained a considerably simplified 2D difference spectrum (ΔS), which exhibits only signals of carbons that are in close proximity to the fluorinated Tyr residues. Fig. 5B shows two representative ω_1 cross sections from the S_0 and ΔS spectra. In the 52.5-ppm cross section, the A24 Cα-CO cross peak and the M1 Cα-CO cross peak exhibit S/S_0 values of 0.73 ± 0.11 and 0.35 ± 0.08, respectively, indicating sizeable dipolar coupling of A24 and M1 Cα to the nearest fluorine, which is 3F-Y3. When multiple cross peaks for the same Cα site are

observed, such as the A34 Cα-CO and Cα-Cβ cross peaks, which both represent dipolar dephasing to the same carbon of A34 Cα, we used the average S/S_0 value to obtain more accurate dipolar dephasing values. For example, the A34 Cα-CO and Cα-Cβ cross peaks show an average S/S_0 value of 0.75 ± 0.03 at 8.4 ms mixing. Similar 2D spectra measured with a shorter REDOR mixing time of 6.4 ms under both 25 kHz and 40 kHz MAS are shown in Fig. S4.

To convert the cross peak intensities in the difference spectrum to quantitative ^{13}C-^{19}F distances, we plotted the S/S_0 values at 6.4 and 8.4 ms mixing times for representative cross peaks (Fig. 6). The Tyr residue that caused the dephasing of a specific Cα atom is assigned based on the known GB1 structure. Clearly different S/S_0 values are observed for different residues, indicating that the experiment is sensitive to different ^{13}C-^{19}F distances. When fitting the measured REDOR decays, we took into account the ^{19}F CSAs and the finite ^{19}F pulse length. We chose not to include pulse imperfections in the simulation for this 3F-Tyr labeled GB1, since the multiple fluorines in this protein cause stronger dipolar dephasing to each ^{13}C, thus offsetting the flip-angle imperfection. In other words, we expect these two systematic uncertainties to partially cancel each other. We simulated the measured decays assuming a two-spin system, thus the extracted distances are apparent values for the statistically mixed fluorination positions 3F (Tyr Hε1) and 5F-Tyr (Hε2). Based on the minimum RMSD between the experimental and simulated REDOR intensities, we obtained best-fit distances of 5.3 Å to 7.7 Å for the cases shown in Fig. 6.

Since the ^{13}C-^{19}F REDOR experiment on the triply 3F-Tyr labeled GB1 is complicated by multi-spin effects and the statistical incorporation of 3F and 5F, we prepared a second fluorinated GB1 containing a single dephasing spin at 5F-Trp43. 2D REDOR-RFDR spectra were measured under 25 kHz MAS (Fig. S5), similar to the conditions for 3F-Tyr GB1. Fig. 7 shows representative ^{13}C-^{19}F dipolar dephasing in this sample. REDOR simulations for this sample include not only ^{19}F CSA and finite-pulse length effects but also ^{19}F flip-angle distributions of 15°, as used for formyl-MLF, giving best-fit distances indicated in Fig. 7.

Fig. 8 summarizes the results of these REDOR experiments on the two fluorinated GB1 samples. For 3F-Tyr GB1, we color-code residues in the protein structure according to the extent of ^{13}C-^{19}F dipolar dephasing measured at the mixing time of 8.4 ms (Fig. 8A). It can be seen that a number of residues near Y3 and Y45 are strongly coupled to the fluorines, with S/S_0 values below 0.55 (red) and between 0.55 and 0.80 (orange). For example, A20, V21, M1 and Q2 are strongly dephased by Y3, while D46 and T51 are significantly dephased by Y45 (Fig. 8B). In the 3F-Tyr-GB1 sample, ten residues belong to the category of having significant difference intensities and hence have short distances to fluorines. Another 12 residues exhibit S/S_0 values greater than 0.80 (grey), indicating either longer distances or proximity to a dynamic fluorine. Selected cross sections for these residues are shown in Fig. S6. We found that residues near Y33, which has a motionally averaged ^{19}F CSA (Fig. S1), show weaker REDOR dephasing, suggesting motional averaging of the ^{13}C-^{19}F dipolar coupling. When motion can be excluded based on the ^{19}F CSA, then even residues with limited dipolar dephasing provide important structural information, by giving lower-bound distances to the ^{19}F atoms. Another 28 residues of GB1 do not have fully resolved signals in the control 2D S_0 spectrum and the difference ΔS spectrum, thus do not

allow distance quantification (cyan). Although GB1 is a microcrystalline protein, at the long REDOR mixing time used, ^{13}C T_2 relaxation reduces spectral sensitivity, thus the spectra were processed using window functions that favor higher sensitivity, resulting in lower resolution than a simple 2D RFDR spectrum. Finally, the six aromatic residues have ^{13}C at natural abundance and thus are excluded from the distance analysis. Fig. 8C highlights the positions of residues that are strongly dephased by 5F-Trp43. In this singly fluorinated sample, it can be clearly seen that many residues within 6–9 Å of 5F-Trp43 show significant dipolar dephasing, thus verifying the effectiveness of the 2D REDOR-RFDR technique for measuring distance constraints in the hydrophobic core of proteins.

Fig. 8D plots all measured ^{13}C-^{19}F distances against the distances read off from the GB1 structure (PDB code: 2LGI). For the Tyr-labeled sample, we use the average distance to 3F and 5F to represent the PDB distances. The further away a carbon is from the fluorinated Tyr, the better the approximation, while for carbons close to a Tyr, the two distances can differ significantly if the aromatic ring is asymmetrically positioned relative to the carbon (Fig. 8B). Y33 has a motionally averaged ^{19}F CSA (Fig. S1), suggesting that this sidechain may undergo rapid two-site jumps. For ^{13}C-labeled residues whose dipolar dephasing is attributed to Y33, we used the CSA reduction factor of 0.76 as the approximate order parameter for the ^{13}C-^{19}F dipolar coupling, and correspondingly shortened the apparent measured distances by a factor of $0.76^{1/3} = 0.91$. For 5F-Trp43 labeled GB1, the ^{19}F sideband spectrum (Fig. S1) indicates a CSA of +46.6 ppm, which is scaled by a factor of 0.87 from the rigid-limit CSA of +53.7 ppm for amino acid 5F-Trp (Roos et al. 2018). We thus decreased the measured apparent distances by $0.87^{1/3} = 0.95$ to obtain truer distances. With these corrections, we obtained a slope of 1.12 for the correlation and a root-mean-square deviation of 0.88 Å between the measured and predicted distances, indicating overall good agreement with the GB1 structure (Table S2).

Fig. 8E shows the *random* uncertainties of the measured distances at 95% confidence intervals (2σ) for the 3F-Tyr GB1 sample, propagated from the sensitivities of the S_0 and S spectra. Large upper-bound distance error bars are seen for a number of residues, reflecting the fact that the measured S/S_0 values for various cross peaks at long REDOR mixing times are sufficiently high or have sufficiently large uncertainties that they do not exclude longer distances. An example is shown for T49 Cβ (Fig. 6), whose S/S_0 values correspond to a best-fit distance of 7.7 Å, in excellent agreement with the expected distance in the GB1 structure, but the sensitivity is insufficient to cap the distance upper limit. In reality, since *systematic* uncertainties such as flip-angle imperfections, finite pulse-length effects and incomplete ^1H decoupling all increase the measured S/S_0 values, the true S/S_0 value is unlikely to be higher than the measured value, therefore the distance upper limits, after accounting for both random and systematic error sources, should be less than those shown in Fig. 8E.

Although REDOR imperfections tend to increase the apparent observed distances, it is interesting to note that many measured distances are shorter than the predicted distances based on the PDB structure. One source of this discrepancy is the simplifying assumption of a two-spin model in the REDOR simulations, since in reality a particular carbon can be simultaneously dephased by two or more ^{19}F spins. To investigate the extent to which the

two-spin model can bias the distance quantification, we simulated three-spin REDOR curves for a ^{13}C coupled to one fluorine spin that is 6 Å away and a second fluorine spin that is 7 – 11 Å away, with an arbitrary angle of 90° between the two C-F vectors. Fig. 9 shows that when the second C-F distance is 10–11 Å, then the three-spin REDOR curve is indistinguishable from the two-spin REDOR curve for 6 Å. This is expected since the second dipolar coupling is so much weaker than the first coupling that it causes little change to the dephasing curve of the strong coupling. When the second distance is 7 or 8 Å, then the three-spin REDOR curve can be well fit by two-spin REDOR curves for a distance of 5.6 Å or 5.8 Å for mixing times up to 12 ms. Therefore, the systematic error introduced by the two-spin approximation is ±0.4 Å for mixing times shorter than 12 ms. For mixing times longer than 12 ms, the two-spin REDOR curves deviate significantly from the three-spin curves. This suggests that the REDOR dephasing at long mixing times can in principle be used to determine whether a carbon is similarly distanced from two fluorines or is much closer a single fluorine than all other fluorines (Tang et al. 2007).

Application of the 2D REDOR-RFDR experiment to the influenza BM2 TM peptide

To investigate the applicability of this REDOR-RFDR experiment to biologically relevant samples, we measured the 2D REDOR-RFDR spectra of the influenza BM2 TM peptide (Fig. 10). The peptide contains 5-^{19}F-W23 and several ^{13}C, ^{15}N-labeled residues, and was reconstituted into a virus-mimetic lipid bilayer and measured using REDOR mixing times of 4.0 and 6.4 ms. Both Cα-selective (75–35 ppm) and CO-selective (185–165 ppm) 2D spectra were measured (Fig. 10A). Among the ^{13}C, ^{15}N-labeled residues, only H19 Cα shows difference intensities (red) at Cα-CO and Cα-Cβ cross peaks, while S12 and G26 difference signals are absent, indicating that these two residues are far from 5-^{19}F-W23. The ω_1 cross section at 174.7 ppm (Fig. 10B) illustrates the benefit of the 2D experiment for spectral editing: while the ω_1 chemical shift includes contributions from the CO sites of three residues (S12, H19, and G26), the difference spectrum shows only the H19 CO-Cα cross peak. Based on the measured S/S_0 values at 4.0 ms and 6.4 ms, we obtained a best-fit H19 CO – W23 5F distance of 6.2 Å (Fig. 10C). A weak difference cross peak is also observed for A17 Cα-Cβ, which fit to a distance of 7.5 Å, but the uncertainty indicates that this distance should be interpreted as a lower bound.

These REDOR dephasing values suggest different sidechain structures and packing of BM2-TM in lipid bilayers compared to DHPC detergent micelles. First, the solution NMR structure of DHPC-micelle bound BM2 (PDB code: 2KIX) indicates an average intra-helical G26 ^{13}CO – W23 5-^{19}F distance of 6.8 Å (Wang et al. 2009) and an average nearest-neighbor inter-helical distance of 8.0 Å. These distances are expected to cause significant dipolar dephasing of G26 by 5F-W23, thus the absence of a difference cross peak for G26 CO strongly suggest that the W23 sidechain structure in bilayer-bound BM2 differs from its structure in the detergent-bound peptide. Second, the measured H19 CO distance of 6.2 Å to 5-^{19}F-W23 is significantly shorter than the average intra-helical distance of 7.9 Å and the average inter-helical distance of 8.3 Å in the solution NMR structure. This observation further supports the notion that the W23 rotameric structure and the helix-helix interface structure in membrane-bound BM2-TM may differ from those of detergent-bound BM2.

Our previous SSNMR experiments showed that membrane-bound BM2-TM proton channels have different pK_a's for the proton-selective H19 from the pK_a's of the proton-selective H37 in influenza A M2 (Williams et al. 2016). This difference was proposed to result from the presence of a second histidine, H27, in BM2, which is located at the membrane-water interface (Williams et al. 2017). With two titratable histidines in the BM2 TM domain, the sidechain structure of the proton-selective H19 may differ from that of H37 in AM2. The ^{13}C-^{19}F distance data shown here will help to elucidate the structural differences between AM2 and BM2 proton channels, to understand how the second histidine impacts proton conduction, and how the membrane environment affects the oligomeric structure of this family of canonical proton channels.

Conclusion

The present data show that multiple ^{13}C-^{19}F distances in the 5–10 Å range can be measured rapidly in fluorinated proteins and peptides under fast MAS in high magnetic fields. The 2D REDOR-RFDR ^{13}C-^{19}F experiment provides site-resolved distances between ^{13}C-labeled residues and a few fluorinated residues in a protein. Our data indicate that the 2D S_0 and S spectra can be measured reliably to give difference spectra, whose cross peak intensities reflect distances after taking into account ^{19}F CSA and the finite pulse-length effect under fast MAS. The precision of the extracted distances chiefly depends on whether multiple fluorines are close together in space to cause multi-spin dipolar dephasing. In GB1 the three 3F-Tyr residues are separated by 6.7–16.3 Å from each other (calculated as the average of all 3F/5F combinations for Tyr pairs). For structurally unknown proteins, these inter-fluorine distances can be independently measured using 2D ^{19}F-^{19}F spin diffusion or dipolar recoupling experiments (Roos et al. 2018). For GB1, we assigned the ^{19}F spins that dephased each carbon based on the known structure of the protein. For *de novo* structure determination, the ^{19}F dephasers can be assigned biosynthetically, by introducing one ^{19}F at a time, by selective inversion of one of the ^{19}F signals, or by a joint and iterative analysis of the ^{19}F-^{19}F and ^{13}C-^{19}F dipolar coupling data.

This 2D ^{13}C-^{13}C resolved ^{13}C-^{19}F REDOR technique can readily incorporate other dipolar recoupling or spin diffusion schemes for ^{13}C-^{13}C correlation, and can be extended to 3D, for example adding a ^{1}H dimension, to further enhance site resolution. The 2D ^{13}C-^{13}C resolved ^{13}C-^{19}F distance measurement approach is conceptually similar to the 2D ^{13}C-^{15}N resolved ^{19}F-^{15}N REDOR technique, which has been demonstrated at 11.7 Tesla (500 MHz ^{1}H Larmor frequency) under 11 kHz MAS (Graesser et al. 2007). The main advantage of the ^{13}C-^{13}C resolved ^{13}C-^{19}F technique is the 1.4-fold longer distances compared to ^{15}N-^{19}F distances for the same coupling strength. A practical benefit is that the REDOR-RFDR experiment can be conducted using a triple-resonance HFC probe while the ^{13}C-^{15}N resolved ^{15}N-^{19}F REDOR requires a quadruple-resonance HFCN probe. It is worth noting that for low-sensitivity biological macromolecules, even a single 2D REDOR-RFDR difference spectrum, measured at one REDOR mixing time, already gives powerful structural constraints about the ^{19}F-proximal residues in proteins. Finally, for proteins in which Tyr residues are the targets of fluorination, labeling both 3-^{19}F and 5-^{19}F will be advantageous over single 3-^{19}F or 5-^{19}F labeling (Ravichandran et al. 2013), by increasing the number of dephasing spins and simplifying distance analysis.

Supplementary Material

Refer to Web version on PubMed Central for supplementary material.

Acknowledgement

The authors thank Dr. Matthias Roos for useful discussions. This work is supported by National Institutes of Health grants GM066976 and GM088204 to M.H.

References

Bak M, Nielsen NC (1997) REPULSION, A Novel Approach to Efficient Powder Averaging in Solid-State NMR, J Magn Reson 125:132–139 [PubMed: 9245368]

Bak M, Rasmussen JT, Nielsen NC (2000) SIMPSON: A general simulation program for solid-state NMR spectroscopy, J Magn Reson 147:296–330 [PubMed: 11097821]

Bennett AE, Rienstra CM, Auger M, Lakshmi KV, Griffin RG (1995) Heteronuclear decoupling in rotating solids., J Chem Phys 103:6951–6958

Bennett AE, Rienstra CM, Griffiths JM, Zhen WG, Lansbury PT, Griffin RG (1998) Homonuclear radio frequency-driven recoupling in rotating solids, J Chem Phys 108:9463–9479

Cady SD, Wang T, Hong M (2011) Membrane-dependent effects of a cytoplasmic helix on the structure and drug binding of the influenza virus M2 protein, J Am Chem Soc 133:11572–11579 [PubMed: 21661724]

Cegelski L (2013) REDOR NMR for drug discovery, Bioorg Med Chem Lett 23:5767–5775 [PubMed: 24035486]

Duncan TM (1997) Principal Components of Chemical Shift Tensors: A Compilation. vol Series vol., Second Edition edn. The Farragut Press, Madison, WI

Dürr HN, Grage SL, Witter R, Ulrich AS (2008) Solid state ^{19}F NMR parameters of fluorine-labeled amino acids. Part I: Aromatic substituents, J Magn Reson 191:7–15 [PubMed: 18155936]

Franks WT et al. (2005) Magic-angle spinning solid-state NMR spectroscopy of the beta 1 immunoglobulin binding domain of protein G (GB1): N-15 and C-13 chemical shift assignments and conformational analysis, J Am Chem Soc 127:12291–12305 [PubMed: 16131207]

Ghosh M, Rienstra CM (2017) H-1-Detected REDOR with Fast Magic-Angle Spinning of a Deuterated Protein, J Phys Chem B 121:8503–8511 [PubMed: 28816462]

Goetz JM et al. (1999) Investigation of the binding of fluorolumazines to the 1-MDa capsid of lumazine synthase by 15N{19F} REDOR NMR, J Am Chem Soc 121:7500–7508

Graesser DT, Wylie BJ, Nieuwkoop AJ, Franks WT, Rienstra CM (2007) Long-range F-19-N-15 distance measurements in highly-C-13, N-15-enriched solid proteins with F-19-dephased REDOR shift (FRESH) spectroscopy, Magn Reson Chem 45:S129–S134 [PubMed: 18157807]

Gullion T, Schaefer J (1989) Rotational-echo double-resonance NMR, J Magn Reson 81:196–200

Hong M, Griffin RG (1998) Resonance Assignment for Solid Peptides by Dipolar-Mediated 13C/15N Correlation Solid-State NMR, J Am Chem Soc 120:7113–7114

Hong M, Schmidt-Rohr K (2013) Magic-Angle-Spinning NMR techniques for measuring long-range distances in biological macromolecules, Acc Chem Res 46:2154–2163 [PubMed: 23387532]

Jaroniec CP, Tounge BA, Rienstra CM, Herzfeld J, Griffin RG (2000) Recoupling of Heteronuclear Dipolar Interactions with Rotational-Echo Double-Resonance at High Magic-Angle Spinning Frequencies, J Magn Reson 146:132–139 [PubMed: 10968966]

Kim SJ, Cegelski L, Preobrazhenskaya M, Schaefer J (2006) Structures of Staphylococcus aureus cell-wall complexes with vancomycin, eremomycin, and chloroeremomycin derivatives by 13C{19F} and 15N{19F} rotational-echo double resonance, Biochemistry 45:5235–5250 [PubMed: 16618112]

Lehninger AL, Nelson DL, Cox MM (1993) Principles of Biochemistry. vol Series vol., 2nd edn Worth Publishers, New York

Luo W, Cady SD, Hong M (2009) Immobilization of the Influenza A M2 Transmembrane Peptide in Virus-Envelope Mimetic Lipid Membranes: A Solid-State NMR Investigation, Biochemistry 48:6361–6368 [PubMed: 19489611]

Mani R, Cady SD, Tang M, Waring AJ, Lehrer RI, Hong M (2006a) Membrane-dependent oligomeric structure and pore formation of a beta-hairpin antimicrobial peptide in lipid bilayers from solid-state NMR, Proc Natl Acad Sci USA 103:16242–16247 [PubMed: 17060626]

Mani R, Tang M, Wu X, Buffy JJ, Waring AJ, Sherman MA, Hong M (2006b) Membrane-bound dimer structure of a b-hairpin antimicrobial peptide from rotational-echo double-resonance solid-state NMR, Biochemistry 45:8341–8349 [PubMed: 16819833]

Pan Y, Gullion T, Schaefer J (1990) Determination of C-N internuclear distances by rotational-echo double-resonance NMR of solids, J Magn Reson 90:330

Ravichandran KR, Liang L, Stubbe J, Tommos C (2013) Formal reduction potential of 3,5-difluorotyrosine in a structured protein: insight into multistep radical transfer, Biochemistry 52:8907–8915 [PubMed: 24228716]

Rienstra CM et al. (2002) De novo determination of peptide structure with solid-state magic-angle spinning NMR spectroscopy, Proc Natl Acad Sci USA 99:10260–10265 [PubMed: 12149447]

Roos M, Wang T, Shcherbakov AA, Hong M (2018) Fast Magic-Angle-Spinning F-19 Spin Exchange NMR for Determining Nanometer Distances in Proteins and Pharmaceutical Compounds, J Phys Chem B 122:2900–2911 [PubMed: 29486126]

Sack II, Goldbourt A, Vega S, Buntkowsky G (1999) Deuterium REDOR: principles and applications for distance measurements., J Magn Reson 138:54–65 [PubMed: 10329226]

Sinha N, Hong M (2003) X-1H Rotational-Echo Double-Resonance NMR For Torsion Angle Determination of Peptides, Chem Phys Lett 380:742–748

Sinha N, Schmidt-Rohr K, Hong M (2004) Compensation for Pulse Imperfections in Rotational-Echo Double-Resonance NMR by Composite Pulses and EXORCYCLE, J Magn Reson 168:358–365 [PubMed: 15140448]

Tang M, Waring AJ, Hong M (2007) Phosphate-Mediated Arginine Insertion Into Lipid Membranes and Pore Formation by a Cationic Membrane Peptide from Solid-State NMR, J Am Chem Soc 129:11438–11446 [PubMed: 17705480]

Wang J, Pielak RM, McClintock MA, Chou JJ (2009) Solution structure and functional analysis of the influenza B proton channel, Nat Struct Mol Biol 16:1267–1271 [PubMed: 19898475]

Wi S, Sinha N, Hong M (2004) Long-range ^{1}H-^{19}F distance measurement in peptides by solid-state NMR, J Am Chem Soc 126:12754–12755 [PubMed: 15469252]

Williams JK, Shcherbakov AA, Wang J, Hong M (2017) Protonation equilibria and pore-opening structure of the dual-histidine influenza B virus M2 transmembrane proton channel from solid-state NMR, J Biol Chem 292:17876–17884 [PubMed: 28893910]

Williams JK, Tietze D, Lee M, Wang J, Hong M (2016) Solid-State NMR Investigation of the Conformation, Proton Conduction, and Hydration of the Influenza B Virus M2 Transmembrane Proton Channel, J Am Chem Soc 138:8143–8155 [PubMed: 27286559]

Wylie BJ, Sperling LJ, Nieuwkoop AJ, Franks WT, Oldfield E, Rienstra CM (2011) Ultrahigh resolution protein structures using NMR chemical shift tensors, Proc Natl Acad Sci USA 108:16974–16979 [PubMed: 21969532]

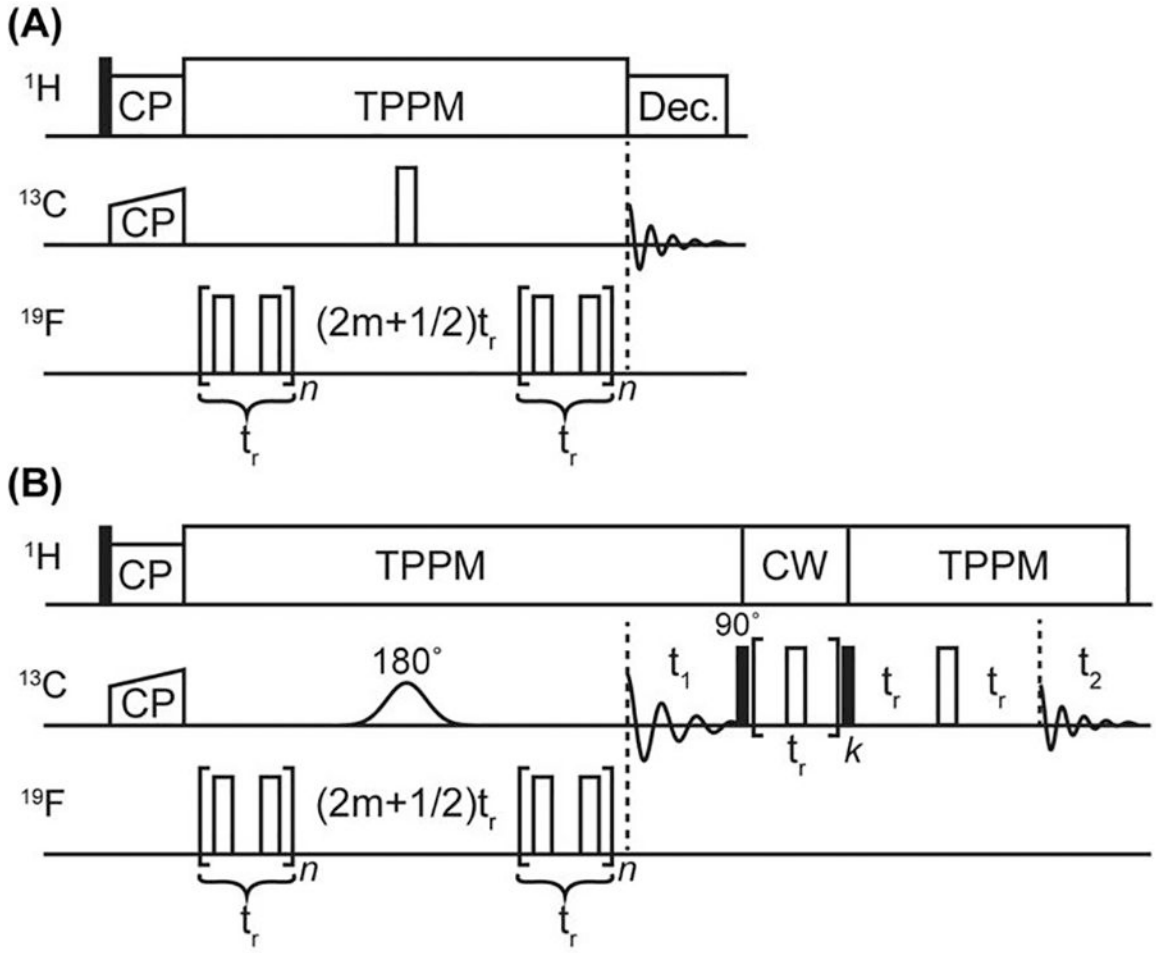

Figure 1.

Pulse sequences used in this study. (**A**) 1D broadband ^{13}C-^{19}F REDOR, conducted at 25 kHz MAS with high power ^{1}H TPPM decoupling during REDOR and ^{13}C detection. Filled and open rectangles represent 90° and 180° pulses, respectively. (**B**) 2D REDOR-RFDR experiment. The ^{13}C selective Gaussian 180° pulse in the middle of the REDOR period uses EXORCYCLE phase cycling. High-power ^{1}H TPPM decoupling was used for 25 kHz MAS. In comparison, the 40-kHz MAS data for GB1 was measured under low-power (10 kHz) WALTZ decoupling.

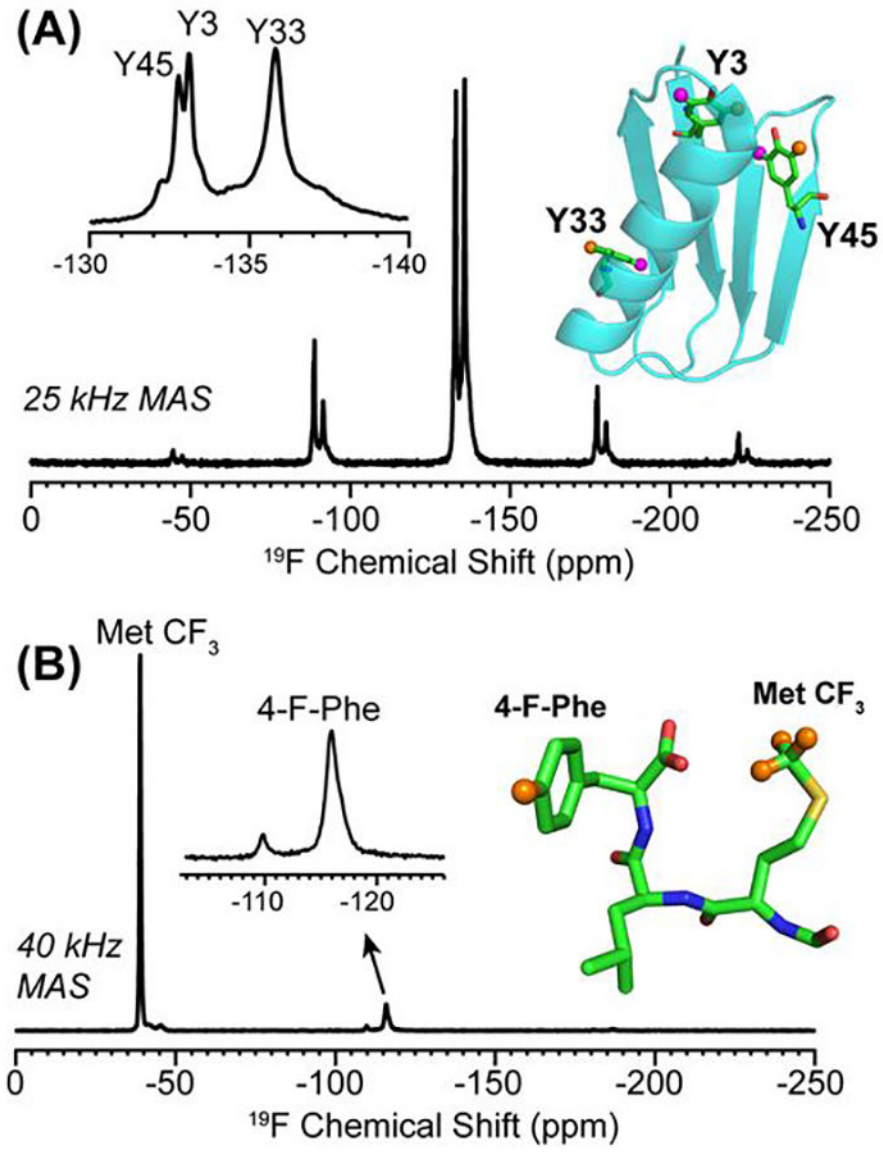

Figure 2.

^{19}F DP MAS spectra of GB1 and formyl-MLF. (**A**) 3F-Tyr GB1 spectrum measured under 25 kHz MAS. The α-helical Y33 peak is well resolved from the β-sheet Y3 and Y45 signals. The Y33 sidechain is mobile, as manifested by weaker sideband intensities compared to the Y3 and Y45. The solid-state NMR structure of GB1 (PDB: 2LGI) is shown, with 3F and 5F positions (orange and magenta) both highlighted. (**B**) Formyl-MLF spectrum measured under 40 kHz MAS. The 4-^{19}F-Phe sideband intensities are largely suppressed at this MAS rate. The solid-state NMR structure of formyl-MLF is shown (PDB: 1Q7O).

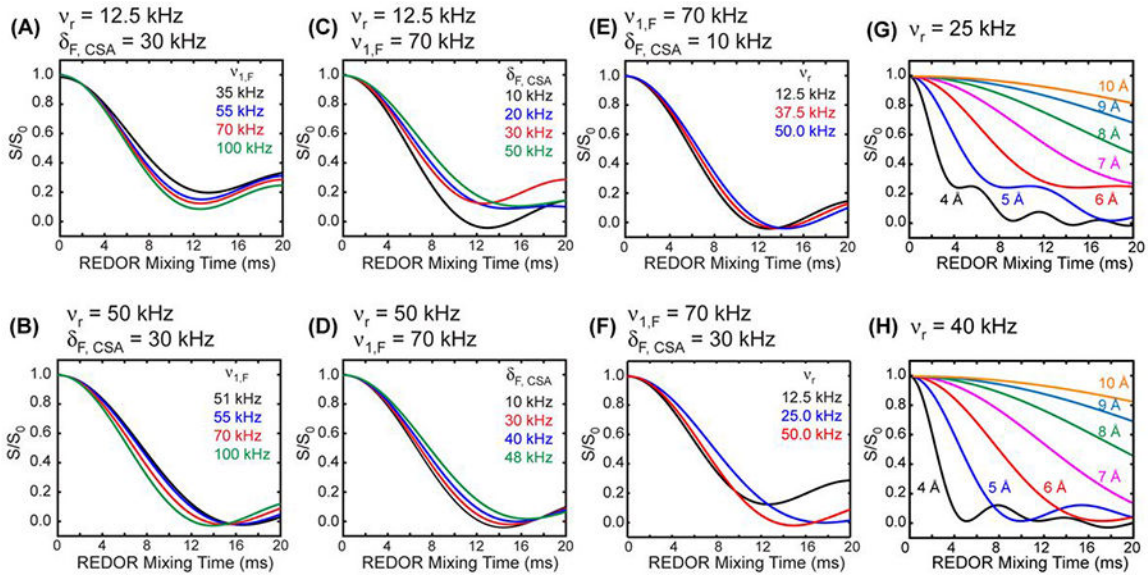

Figure 3.

Simulated ^{13}C-^{19}F REDOR curves for varying ^{19}F rf field strengths, ^{19}F CSA and MAS rates. All simulations are for a 6.0 Å distance with a dipolar coupling constant of 132 Hz. (**A**) When the MAS frequency is smaller than the ^{19}F CSA, weaker ^{19}F rf field strength results in less dipolar couplings and higher REDOR S/S_0 intensities. (**B**) When the MAS frequency exceeds the ^{19}F CSA, weaker ^{19}F rf fields shift the REDOR minimum to longer times but do not raise the S/S_0 values. (**C**) Under slow MAS, large ^{19}F CSAs significantly increase the S/S_0 values and shift the time of the minimum S/S_0 value to longer times, even when strong ^{19}F rf fields are applied. (**D**) When the MAS frequency exceeds the ^{19}F CSA and when high rf fields are applied, the REDOR S/S_0 values are relatively invariant to the CSA. (**E**) For a fixed ^{19}F rf field of 70 kHz and a small ^{19}F CSA of 10 kHz, MAS frequencies from 12.5 to 50 kHz cause little difference in REDOR dephasing. (**F**) For a fixed ^{19}F rf field strength of 70 kHz and a large ^{19}F CSA of 30 kHz, a slow MAS rate of 12.5 kHz causes incomplete REDOR dephasing, while 25 kHz and 50 kHz MAS restores REDOR dephasing to the expected minimum, but with different rates. (**G, H**) Simulated ^{13}C-^{19}F REDOR curves for distances from 4 Å to 10 Å under 25 kHz MAS (G) and 40 kHz MAS (H). A ^{19}F CSA of 30 kHz and a ^{19}F rf field strength of 70 kHz were used in the simulations.

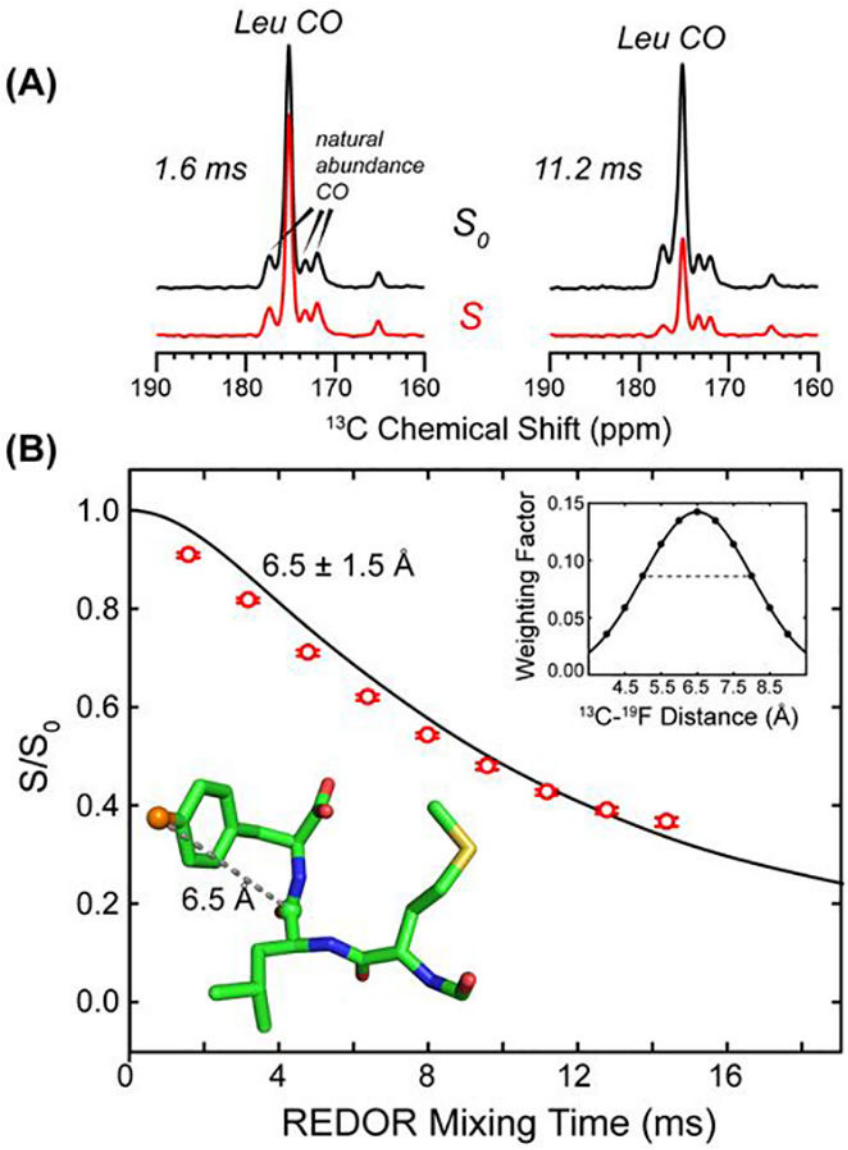

Figure 4.

1D ^{13}C-^{19}F REDOR data of 4F-Phe labeled formyl-MLF under 25 kHz MAS. (**A**) Representative REDOR S_0 and S spectra, measured at mixing times of 1.6 ms (left) and 11.2 ms (right). (**B**) Measured S/S_0 decay (red circles) of Leu ^{13}CO as a function of mixing time. The PDB structure 1Q7O shows the average distance of 6.5 Å between 4-^{19}F Phe and Leu CO. The simulated REDOR curve (black) uses a Gaussian distance distribution as shown in the inset, and takes into account the ^{19}F CSA, ^{19}F finite-pulse lengths, and a pulse flip-angle distribution of 15° around 180°.

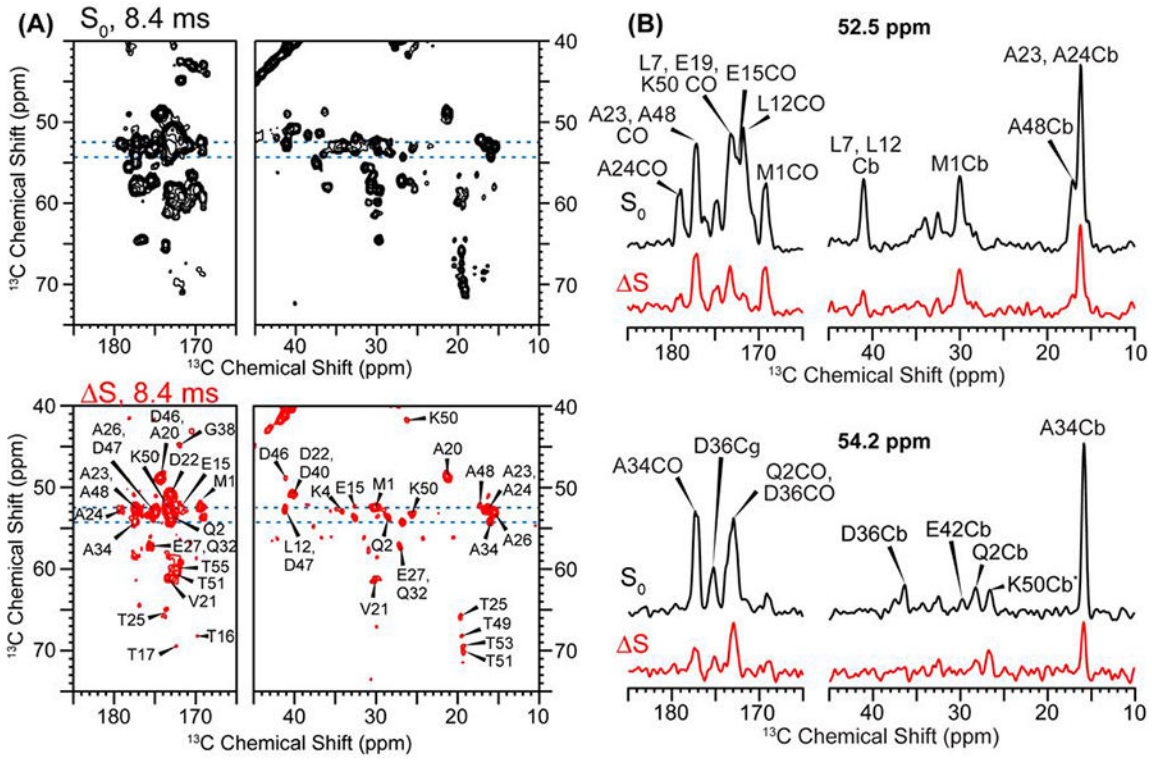

Figure 5.

2D REDOR–RFDR spectra of 3F-Tyr-labeled GB1 measured at 25 kHz MAS. The REDOR mixing time was 8.4 ms and the RFDR mixing time of 2.08 ms. (**A**) Control spectrum (S_0) showing all signals and difference spectrum (ΔS) showing only signals of ^{13}C spins that are close to a fluorinated Tyr. (**B**) Representative ω_1 cross sections from the S_0 and ΔS spectra. The difference spectrum shows fewer peaks, indicating that the experiment can serve as a spectral editing method.

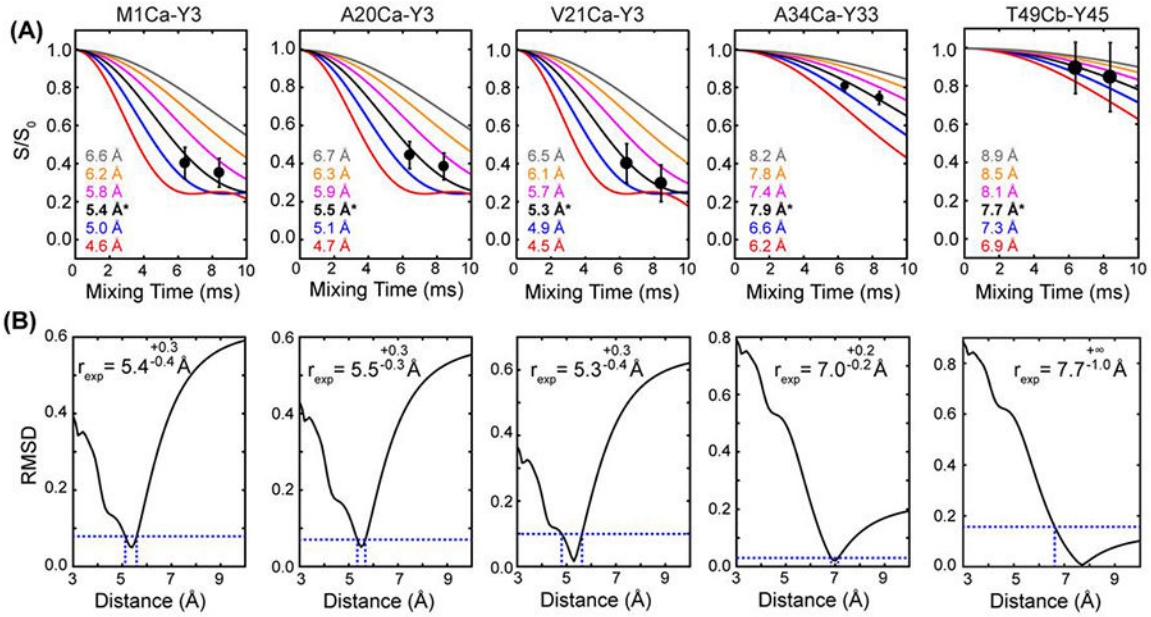

Figure 6.

Representative Cα REDOR S/S_0 decays of 3F-Tyr-labeled GB1 from 2D REDOR-RFDR spectra. (**A**) Measured S/S_0 decays for indicated ^{13}C-^{19}F spin pairs. Two-spin simulations that include ^{19}F CSAs and finite pulse-length effects are overlaid with the data, with the best-fit simulations indicated in black. (**B**) RMSD between the measured and simulated REDOR dephasing. Horizontal blue lines correspond to the average uncertainty of the S/S_0 values propagated from the experimental spectra, below which are distances that agree with the measured REDOR intensities.

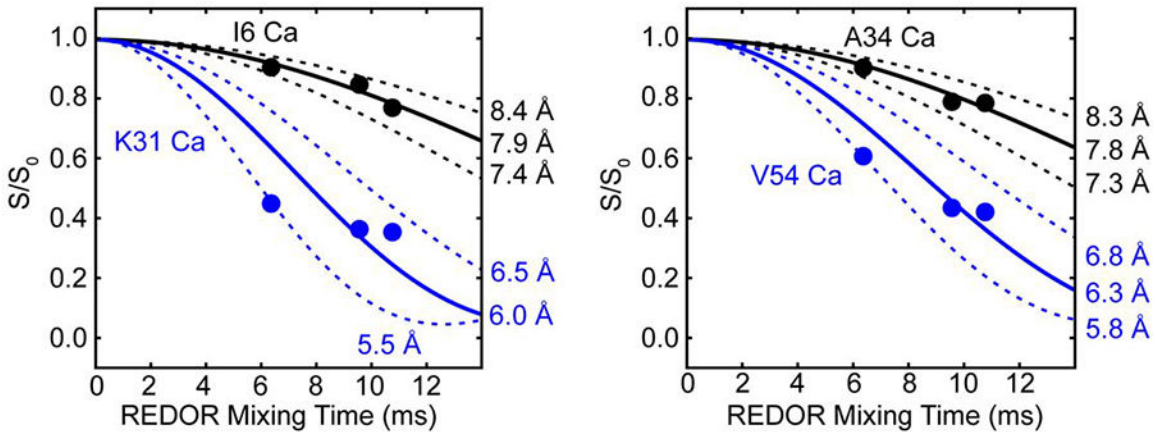

Figure 7.

Representative Cα-F S/S_0 decays of 5F-Trp43-labeled GB1, extracted from 2D REDOR-RFDR spectra measured under 25 kHz MAS. Single-distance REDOR simulations incorporated the ^{19}F CSA, finite pulses, and a flip-angle distribution of ±15°.

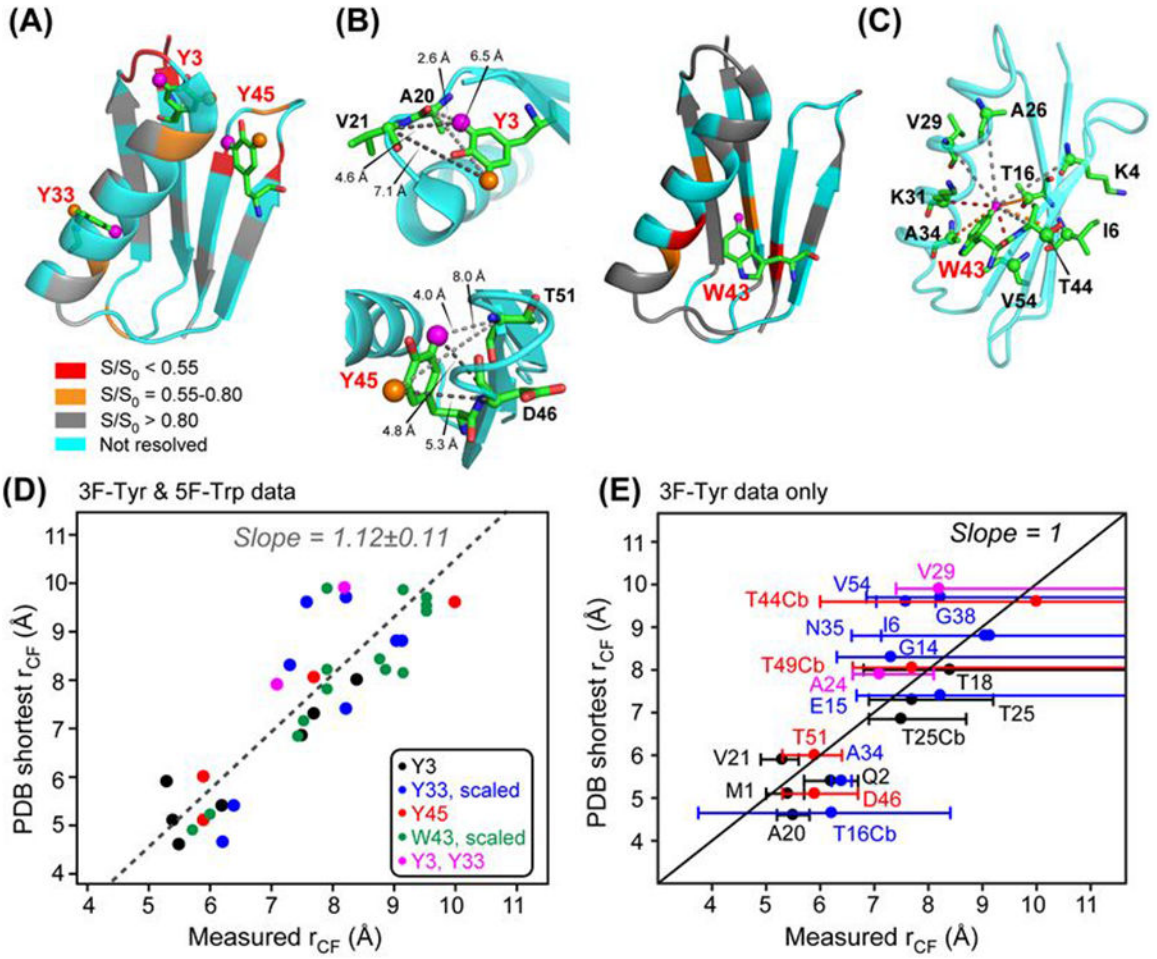

Figure 8.

^{13}C-^{19}F distance measurement and quantification in GB1. (**A**) Solid-state NMR structure of GB1 (PDB code: 2LGI), showing the positions of the three Tyr residues. Residues whose carbons show significant REDOR dephasing at 8.4 ms are color-coded. Cyan residues have S_0 signals that are not sufficiently resolved. (**B**) Zoomed-in regions around Y3 and Y45, showing several residues with significant ^{13}C-^{19}F dipolar dephasing. For A20 Cα, V21 Cα, and T51 Cα, distances to the 3F (magenta) and 5F (orange) positions of Y3 and Y45 differ significantly, thus the measured REDOR dephasing is an average of two distances. In comparison, D46 Cα has similar distance of 4.8 and 5.3 Å to Y45 3F and 5F. (**C**) GB1 structure showing the position of 5F-Trp43. Residues that exhibit significant ^{13}C-^{19}F dephasing are indicated. (**D**) Comparison of measured and predicted ^{13}C-^{19}F distances. The y-axis shows the shortest distance of a carbon to one of the three 3F-Tyr residues and to 5F-Trp43. The measured distances that are assigned to Y33 and W43 were corrected for sidechain dynamics using the measured CSA order parameters. Residues are color-coded according to the fluorinated aromatic residue that dephases the carbon. Magenta symbols indicate two residues (V29 and A24) with similar distances to Y3 and Y33. The measured and predicted distances correlate with a slope of 1.12. (**E**) Measured Tyr-dephased ^{13}C-^{19}F distances with associated random uncertainties due to spectral sensitivity. Large distance upper-bounds result from limited sensitivity of some of the cross peaks at long REDOR

mixing times, which do not permit exclusion of long distances. This random uncertainty is expected to be significantly offset by systematic uncertainties. A slope-1 line guides the eye for the ideal correlation between measured and predicted distances.

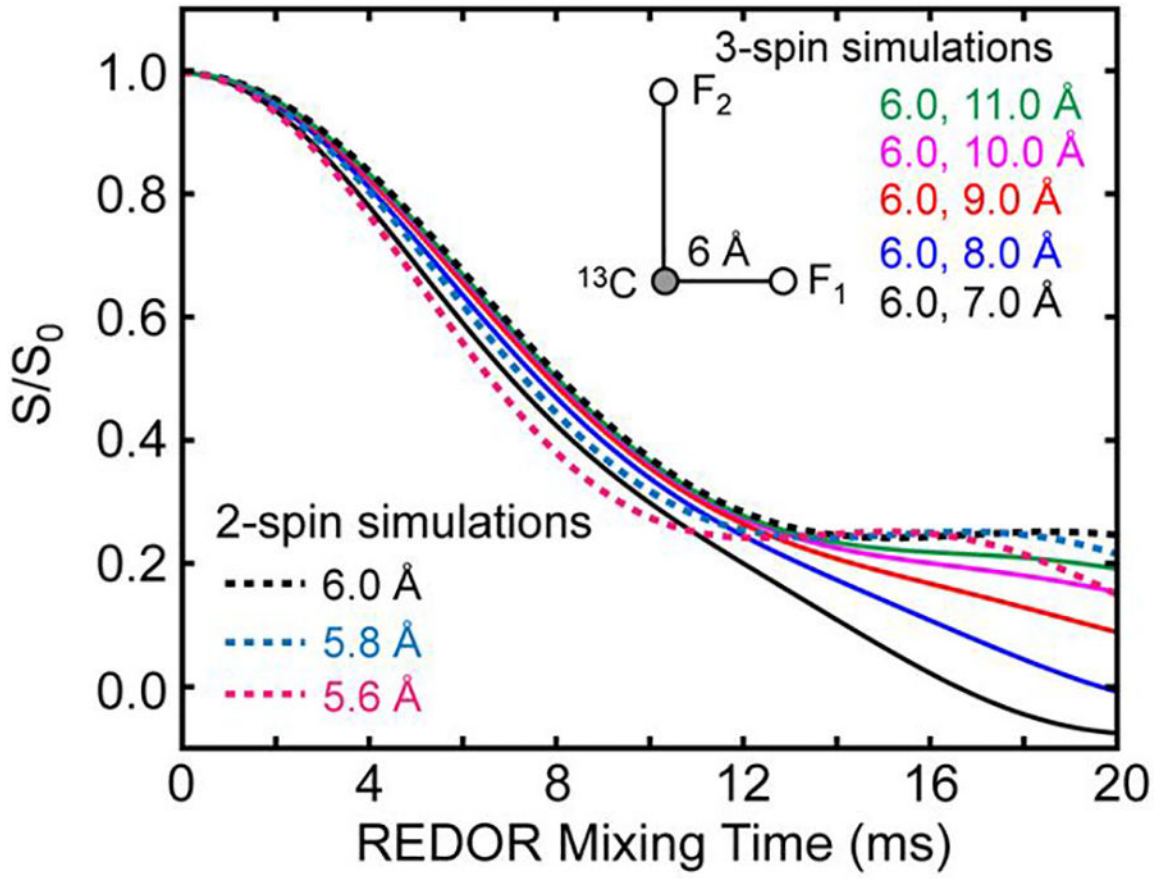

Figure 9.

Simulated ^{13}C-^{19}F REDOR curves to investigate the applicability of two-spin simulations to approximate three-spin systems containing one carbon and two fluorines (F1 and F2). The three-spin simulations used a C-F1 distance of 6 Å and a variable C-F2 distance from 7 Å to 11 Å, with an arbitrary angle of 90° between the two vectors. The two-spin REDOR curve approximates the three-spin REDOR curve for mixing times up to ~12 ms when the C-F2 distances are longer than 7 Å. These simulations used a ^{19}F CSA of −75 ppm, a ^{19}F rf field strength of 71 kHz, and an MAS rate of 25 kHz.

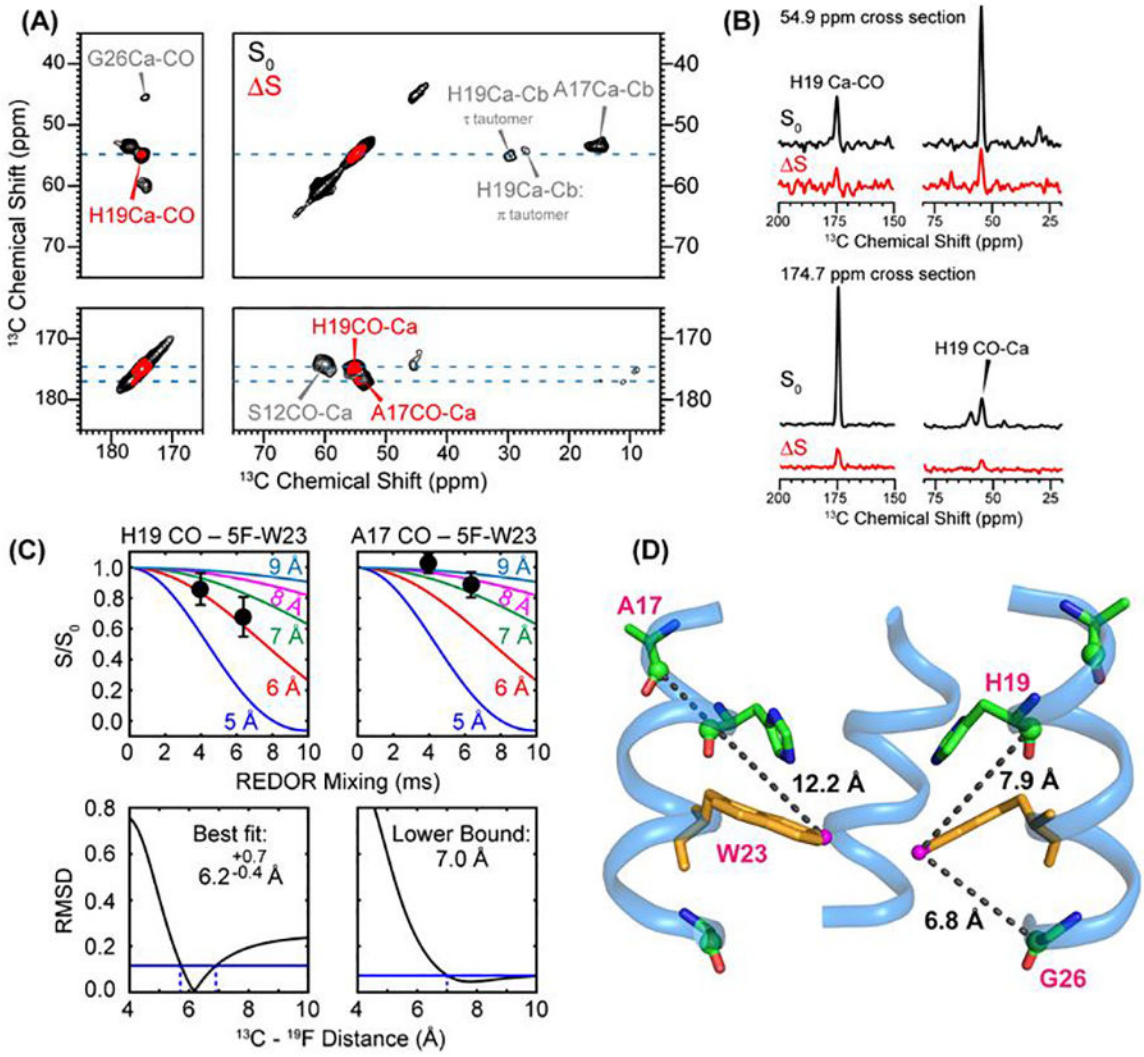

Figure 10.

2D resolved ^{13}C-^{19}F REDOR data of membrane-bound BM2 TM peptide containing 5F-Trp23. The spectra were measured under 25 kHz MAS with a REDOR mixing time of 6.4 ms and a RFDR mixing time of 2.0 ms. (**A**) 2D S_0 spectrum (black) overlaid with the ΔS spectrum (red). Only H19 shows significant difference intensities, indicating that only H19 is near 5-^{19}F-W23. (**B**) Selected cross sections of the 6.4 ms REDOR-RFDR 2D spectra. H19 CO and Cα both show significant dipolar dephasing while S12 CO and A17 CO have negligible dephasing. (**C**) Measured S/S_0 values of H19 and A17 CO from the CO-selective 2D spectra, overlaid with simulated REDOR curves. The RMSD between the measured and simulated S/S_0 values are shown below the data. Best-fit simulations give a distance of 6.2 Å between H19 CO and W23 5-^{19}F. The shallow minimum in the A17 CO RMSD curve suggests a distance of ~7.5 Å from 5-^{19}F-W23. (**D**) Solution NMR structure of DHPC-bound BM2 (PDB code: 2KIX), showing average intra-helical distances of H19 CO, G26 CO, and A17 CO to 5-^{19}F-W23. The H19-W23 distances are too long compared to the data, while the G26-W23 distances are too short compared to the data.